

Thrust Production in Highly Flexible Pectoral Fins: A Computational Dissection

AUTHORS

Srinivas Ramakrishnan¹
ANSYS, Inc.

Meliha Bozkurttas
Franklin W. Olin
College of Engineering

Rajat Mittal
Department of Mechanical Engineering,
Johns Hopkins University

George V. Lauder
Department of Organismic
and Evolutionary Biology,
Harvard University

Introduction

Robust design based on natural systems is a significant engineering challenge. Evolution-based design is inherently a multi-objective optimization problem. Natural selection puts pressure on organisms to produce locomotion abilities that balance competing requirements of speed, efficiency, and effectiveness. The goals of ongoing research efforts are to elucidate the competing requirements that have enabled the evolution of highly maneuverable propulsion/locomotion at low speeds. Prominent natural systems of interest are flapping flight in air and aquatic locomotion and a common feature among these systems is the presence of highly compliant control surfaces. Organisms that employ these models of locomotion appear to exploit the flexibility of their wings/

¹Work presented here was done while the author was a postdoctoral scientist at The George Washington University prior to joining Ansys Inc.

ABSTRACT

Bluegill sunfish pectoral fins represent a remarkable success in evolutionary terms as a means of propulsion in challenging environments. Attempts to mimic their design in the context of autonomous underwater vehicles have overwhelmingly relied on the analysis of steady swimming. Experimental observations of maneuvers reveal that the kinematics of fin and wake dynamics exhibit characteristics that are distinctly different from steady swimming. We present a computational analysis that compares, qualitatively and quantitatively, the wake hydrodynamics and performance of the bluegill sunfish pectoral fin for two modes of swimming: steady swimming and a yaw turn maneuver. It is in this context that we comment on the role that flexibility plays in the success of the pectoral fin as a versatile propulsor. Specifically, we assess the performance of the fin by conducting a “virtual dissection” where only a portion of fin is retained. Approximately 90% of peak thrust for steady swimming is recovered using only the dorsal half. This figure drops to 70% for the yaw turn maneuver. Our findings suggest that designs based on fin analysis that account for various locomotion modes can lead to more robust performance than those based solely on steady swimming.

Keywords: computational fluid dynamics (CFD), immersed boundary methods (IBM), bluegill sunfish, biological locomotion

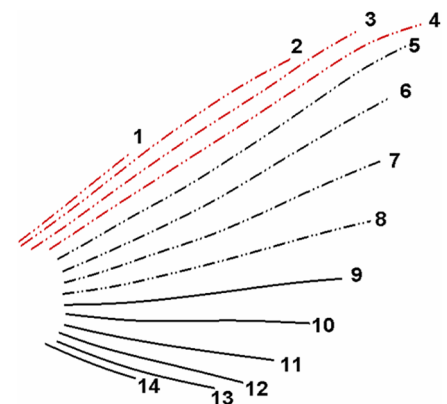
fins to achieve high maneuverability at low speeds. This paper presents the analysis of one such control surface: the bluegill sunfish pectoral fin.

A typical sunfish pectoral fin consists of 14 fin rays as shown in Figure 1. We see the fin rays numbered sequentially starting from the dorsal edge (ray 1) to the ventral edge (ray 14). These rays support an asymmetric planform shape for the pectoral fin. Figure 3 shows different frames of the sunfish executing a maneuver from a ventral view. The motion of the pectoral fin and body are captured using multiple high-speed video cameras simultaneously operating at 250 or more frames per second with a 1024 × 1024 resolution (Lauder et al., 2006). The wing surface is digitized at about 300 spatial locations at several points

during the fin cycle. Thus, the kinematics of the fin motion is acquired for the simulation. The collaboration with experimentalists (biologists and

FIGURE 1

Bluegill sunfish pectoral fin consists of 14 rays, which form the full planform. The dissected planform is interpolated from rays 1–8 to investigate the flow and performance.



engineers), through a multi-disciplinary effort (Lauder et al., 2006; Mittal et al., 2006), has enabled high-fidelity data to be used in the computational analysis (see Figure 2).

It is clear from looking at the fin motion during the maneuver (see Figure 3) that the kinematics of the fin involves both deformation and translation. This poses severe challenges for traditional body-fitted computational methods. Here, the immersed boundary method, with its ability to handle complex deforming structures, enables us to undertake high-fidelity computa-

tional fluid dynamics (CFD) analysis of the pectoral fin hydrodynamics (see Computational Methodology). It has been used to gain valuable insight into pectoral fin hydrodynamics in steady swimming (Bozkurttas et al., 2009; Dong et al., 2010). The experimentally obtained steady swimming kinematics was analyzed, and an efficient reconstruction of the kinematics using proper orthogonal decomposition (POD) was obtained. The POD modes using a combination of the first three modes (hereafter referred to as Mode 1 + 2 + 3) were successful in reproducing two

thirds of the full fin kinematics. More significantly, this combination of modes was found to retain 92% of the thrust produced using the actual kinematics (Bozkurttas, 2007; Bozkurttas et al., 2009). Further, detailed analysis of the pressure distribution over the full fin surface (rays 1-14) during steady swimming also revealed that most of the thrust was produced by the dorsal part mainly around the spanwise tip region (Bozkurttas et al., 2009; Dong et al., 2010) (see Figure 5). Since different sections of the pectoral fin trace different trajectories during a fin stroke, the contribution of each region of the fin to its overall performance may not be uniform. Naturally, this leads us to the central theme of this paper, the idea of examining the thrust production of different sections of the fin. The goal is to enable a virtual “dissection” or “ablation” of the pectoral fin dynamics and the effect of this ablation on the fin performance. It is expected that this will yield useful insight into the hydrodynamic function of the fin in various swimming modes.

FIGURE 2

Bioinspired design paradigm.

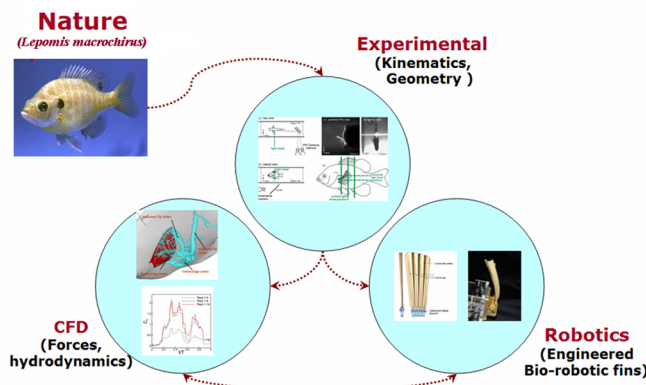
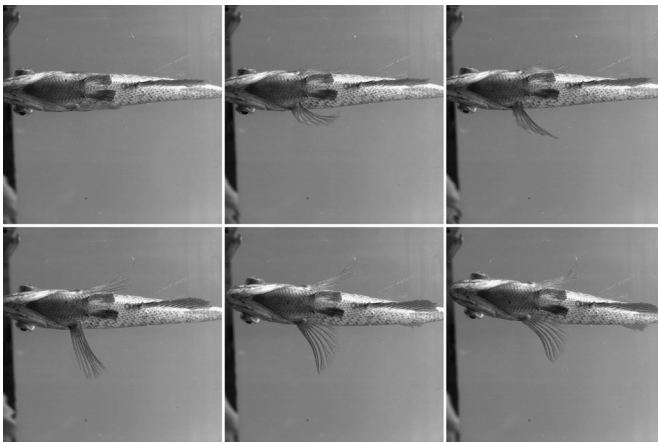


FIGURE 3

A bluegill sunfish during a maneuver: ventral (bottom) view. Images are frames from a high-speed video. Note the differential motion of the left and right side fins. Top row: $t/T = 0$, $t/T = 0.23$, $t/T = 0.30$. Bottom row: $t/T = 0.46$, $t/T = 0.70$, $t/T = 0.84$.



Computational Methodology

We present a brief description of the Cartesian grid-based immersed boundary method for moving boundaries starting with the governing equations. The three-dimensional unsteady, viscous incompressible Navier-Stokes equations are given as

$$\begin{aligned} \frac{\partial u_i}{\partial x_i} &= 0 \\ \frac{\partial u_i}{\partial t} + \frac{\partial (u_i u_j)}{\partial x_j} &= -\frac{1}{\rho} \frac{\partial p}{\partial x_i} + \nu \frac{\partial}{\partial x_j} \left(\frac{\partial u_i}{\partial x_j} \right) \end{aligned} \quad (1)$$

where $i, j = 1, 2, 3$, u_i are the velocity component, p is the pressure, and ρ

and ν are the fluid density and kinematic viscosity. We have employed a conventional notation where repeated indices imply summation.

1. Numerical Method

The Navier-Stokes equations (Eq. 1) are discretized using a cell-centered, collocated (non-staggered) arrangement of the primitive variables (\mathbf{u}_i, p). In addition to the cell-centered velocities (\mathbf{u}_i), the face-centered velocities, U_i , are computed. A second-order Adams-Bashforth scheme is employed for the convective terms while the diffusion terms are discretized using an implicit Crank-Nicolson scheme which eliminates the viscous stability constraint. The spatial derivatives are computed using a second-order accurate central difference scheme. The equations are integrated in time using the fractional step method (Chorin, 1967). In the first sub-step of this method, a modified momentum equation is solved and an intermediate velocity \mathbf{u}^* obtained. The second sub-step requires the solution of the pressure correction equation which is solved with the constraint that the final velocity \mathbf{u}_i^{n+1} be divergence-free. This gives a Poisson equation for the pressure correction and a Neumann boundary condition imposed on this pressure correction at all boundaries. This Poisson equation is solved with a highly efficient geometric multigrid method which employs a Gauss-Siedel line-SOR smoother. Once the pressure correction is obtained, the pressure and velocity are updated (see Dong et al., 2006 and Mittal et al., 2008, for additional details). These separately updated face velocities satisfy discrete mass conservation to machine accuracy

and use of these velocities in estimating the non-linear convective flux leads to a more accurate and robust solution procedure. The advantage of separately computing the face-centered velocities was initially proposed by Zang et al. (1994) and discussed in the context of the Cartesian grid methods in Ye et al. (1999) and Mittal et al. (2008).

2. Immersed Boundary Treatment

The immersed boundary method used here employs a multi-dimensional ghost cell methodology to impose the boundary conditions on the immersed boundary. The current solver is designed from the start for fast, efficient, and accurate solution of flows with complex three-dimensional, moving boundaries. Also, the current method is a “sharp” interface method in that the boundary conditions on the immersed boundary are imposed at the precise location of the immersed body, and there is no spurious spreading of boundary forcing into the fluid as what usually occurs with diffuse interface methods (Mittal & Iaccarino, 2005).

3. Geometric Representation of Immersed Boundary

The current method is designed to simulate flows over arbitrarily complex 2D and 3D immersed stationary and moving boundaries and the approach chosen to represent the boundary surface should be flexible enough so as not to limit the type of geometries that can be handled. A number of different approaches are available for representing the surface of the immersed boundary, including level sets (Osher & Sethian, 1988; Tran & Udaykumar, 2004), and unstructured surface grids. In the current solver, we choose to represent the surface of

the immersed boundary by an unstructured mesh with triangular elements. This approach is very well suited for the wide variety of engineering and biological configurations that are of interest to us and is compatible with the immersed boundary methodology used in the current solver.

4. Boundary Motion

Boundary motion can be included into immersed boundary formulation with relative ease. In advancing the field equations from time level n to $n + 1$ in the case of a moving boundary, the first step is to move from its current location to the new location. This is accomplished by moving the nodes of the surface triangles with a known velocity. Thus, we employ the following equation to update the coordinates (X_i) of the surface element vertices,

$$\frac{X_i^{n+1} - X_i^n}{\Delta t} = V_i^{n+1} \quad (2)$$

where V_i is the vertex velocity. The vertex velocity can either be prescribed or it can be computed from a dynamical equation if the body motion is coupled to the fluid. The next step is to determine the ghost cells for this new immersed boundary location and recompute interpolation weights associated with the ghost point methodology. Subsequently, the flow equations, which are written in Eulerian form, are advanced in time. The general framework described above can, therefore, be considered as Eulerian-Lagrangian, wherein the immersed boundaries are explicitly tracked as surfaces in a Lagrangian mode, while the flow computations are performed on a fixed Eulerian mesh. Additional

details regarding the current immersed boundary methodology may be found in Mittal et al. (2008).

Computational Setup

All simulations are conducted in a rectangular computational domain. The boundary conditions on the bounding box of the domain are free-stream on the left (x direction), out-flow on the right while the remaining boundaries (top and bottom (y direction) and front and back (z direction)) employ slip boundary conditions (see Figure 4). The fin surface and fish body are considered as no-slip boundaries. The fins are treated as deforming membranes while the body, where applicable, is treated as rigid body undergoing general motion. The Reynolds number in the present work is defined as $Re = UL_s/\nu$ where U , L_s , and ν are the swimming velocity, spanwise fin length, and the kinematic viscosity of

water ($\nu = 1.007 \times 10^{-6} \text{ m}^2 \text{ s}^{-1}$ at room temperature), respectively.

Based on a swimming speed of 1.1 body length per second, the Reynolds number for the steady swimming is 6300. However, a comparison of the force coefficients obtained at $Re = 1440$ with those at the experimental Reynolds number appear to be in good agreement both quantitatively and qualitatively (Bozkurtas, 2007). So, for computational expediency, we use the lower Reynolds number in the steady swimming analysis (Dong et al., 2010). As mentioned earlier, low dimensional model performance analyses have shown that Mode 1 + 2 + 3 gait that accounts for 67% of the fin motion still produces 92% of the thrust (Bozkurtas et al., 2009). Therefore, in lieu of the experimentally extracted fin kinematics, this simplified model has been used here. The grid size in these simulations is $153 \times 161 \times 97$, which is about 2.35 million

grid points. A domain size of $3.8L_s \times 4.5L_s \times 1.8L_s$ is selected where L_s is the span wise size of the fin. Comprehensive studies have been carried out to assess the effect of the grid resolution and domain size on the salient features of the flow and also to demonstrate the accuracy of the selected grid (Bozkurtas, 2007).

The Reynolds number for the turning maneuver based on a freestream velocity of 0.5 body lengths per second is approximately 3500. The domain size employed for the maneuver is $7.5L_s \times 5L_s \times 5L_s$. The pectoral fins and an idealized body, immersed in the computational grid, are shown in Figure 4. The nominal grid size used in the current simulation is $241 \times 145 \times 145$ (see Figure 4). Finally, the domain size for the maneuver with just the strongside (outside) fin is $4L_s \times 4L_s \times 4L_s$ with a non-uniform grid using 128 points in all three dimensions.

We note in passing that all the steady swimming cases and ablated fin simulations (for the maneuver) do not include the fish body. This is reasonable since we have observed that the difference in the thrust coefficients with and without the body is minimal. As we shall see shortly, the wake dynamics for both steady swimming and maneuver are dominated by vortex structures generated far from the fish body (see Figures 5 and 8). Thus, the interaction between the body and the fin hydrodynamics is minimal.

The performance of the fin is evaluated using the computed force coefficients which are defined as,

$$C_T = \frac{2F_x}{\rho U_\infty^2 A_{fin}}; C_L = \frac{2F_y}{\rho U_\infty^2 A_{fin}};$$

$$C_Z = \frac{2F_z}{\rho U_\infty^2 A_{fin}} \quad (3)$$

FIGURE 4

Cartesian grid (4.8 million grid points) and unstructured mesh employed for yaw maneuver: (a) x - y plane section, (b) x - z plane section, (c) y - z plane section (strongside fin on the left and weakside on right of the body), and (d) unstructured surface mesh (pectoral fin only, number of nodes = 10,000, number of elements = 19,602).

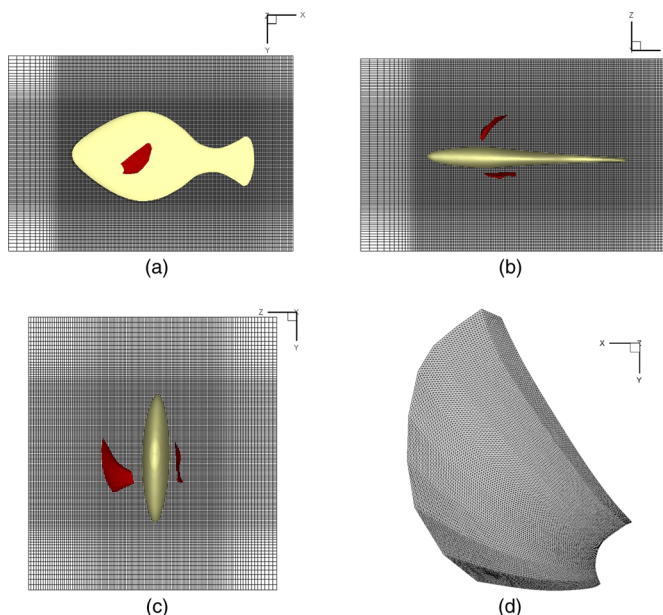
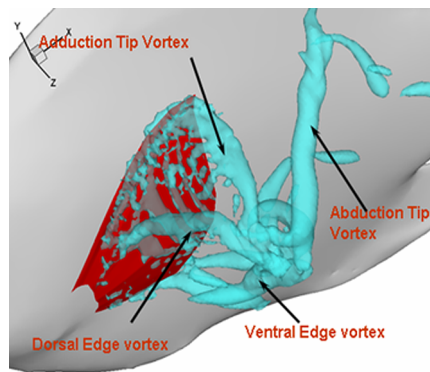


FIGURE 5

The anatomy of the principal vortex dynamics involved in steady swimming.



where F_x , F_y and F_z are the forces respectively in the streamwise (drag/thrust), vertical (lift), and spanwise (lateral) directions, A_{fin} is the nominal fin area, and ρ is the density of the fluid. U_∞ is the forward swimming velocity. The force components are calculated by directly integrating the computed pressure and shear stress on the fin surface.

Results Steady Swimming

A snapshot of the vortex dynamics at the end of a steady swimming fin beat is shown in Figure 5. Note the

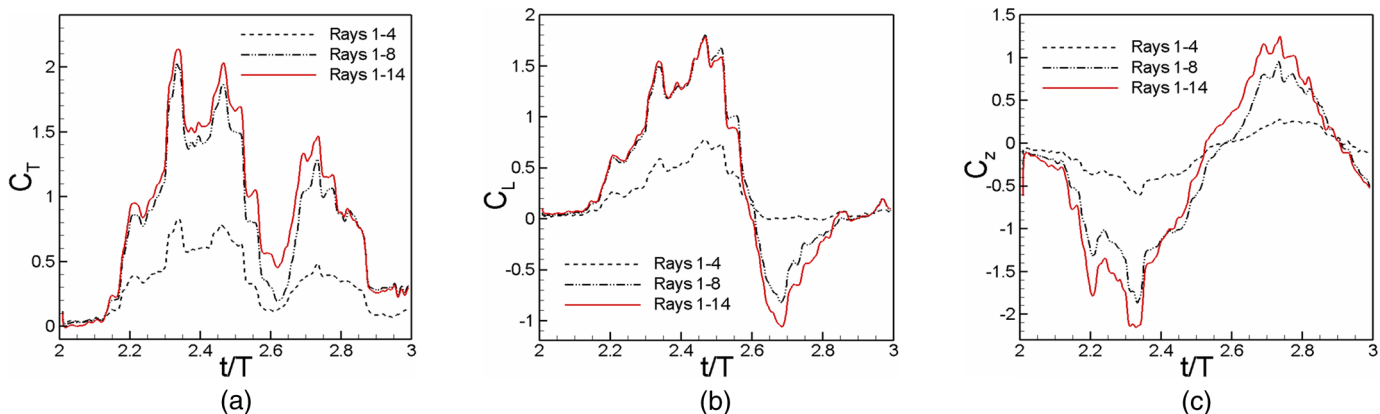
complex interaction of among vortices generated by the path traversed by the fin tip during a fin beat. Clearly, both adduction and abduction appear to produce distinct vortex structures. This is in stark contrast with a simple ring vortex created during the maneuver (see Figure 8). The time variations of the force coefficients (C_T , C_L and C_Z) for three fin planforms are plotted in Figure 6. Note the presence of two distinct and comparable peaks corresponding to the adduction and abduction phases. This force signature bears the trademark of efficiency where the fin sustains net forward thrust throughout its fin beat. Clearly, the chordwise and spanwise compliance of the fin allows the simultaneous formation and persistence of two distinct vortex structures within a single fin beat. A rigid planform would lead to a more restrictive envelope for the fin tip path resulting in vortex dynamics that have stronger interactions detrimental to sustained net thrust production (see Akhtar et al., 2007).

We now construct two different ablated fin models: one that contains only the rays 1-4 and one that contains rays 1-8 (see Figure 1). The motion of these dissected fins is precisely the

same as that for the full fin and we carry out flow simulations for both of these cases. Examining the results from our virtual dissection, we notice that the dorsal half of the fin (rays 1-8) captures the two main peaks of the thrust and preserves 90% of the thrust production of the full fin planform. Consequently, the ventral contribution of the fin, represented by rays 9-14 in Figure 1, to the thrust production is found to be insignificant. Also, the planform interpolated from rays 1-4 has a similar trend in thrust variation during the entire fin-beat cycle albeit with smaller amplitudes. Interestingly, it has two main peaks and even the two local peaks in the abduction phase as in the full fin case. This further reinforces the notion that the dorsal leading edge of the bluegill's pectoral fin dominates the overall performance during steady swimming propulsion. This planform produces almost 40% of the thrust produced by the fish fin while undergoing Mode 1 + 2 + 3 gait. Finally, we observe similar tendencies for lift and spanwise force coefficients for the three planforms, except the case with just rays 1-4 where the values show attenuation. The key observation here is that the dorsal half of the pectoral fin

FIGURE 6

Comparison of time variation of force coefficients for three different fin planforms (rays 1-4, rays 1-8, full planform) at Mode 1 + 2 + 3 gait: (a) streamwise force, (b) vertical force, and (c) lateral force.



(rays 1-8) is responsible for producing a majority of the thrust. These results bring into question the need for the ventral portion of the fin. We explore this in detail as we consider the case of the yaw turn maneuver.

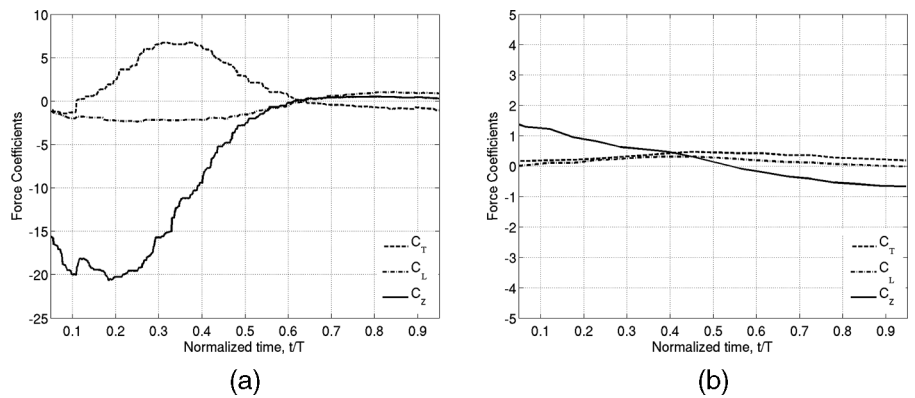
Yaw Turn Maneuver

The evolution of wake structure from the strongside fin, that drives the maneuver, is shown from two vantage points: lateral (Figure 8 (a,c,e)) and dorsal (Figure 8 (b,d,f)). The well-defined vortex ring formed during the outstroke (abduction) produces a lateral jet oriented normal to the fish body (see Figure 9). This type of vortex ring and associated lateral jet shown in Figures 8 and 9 have also been observed in experimental visualization (Drucker & Lauder, 2001). The peak lateral velocity is found to be greater than three times the freestream velocity. Consequently, the lateral forces developed are several times that observed in forward thrust for the steady swimming case (Bozkurttas, 2007). Preliminary estimates for stroke-averaged force coefficients ratio between lateral force in maneuvering ($\overline{C_Z} = 6.1$) to steady swimming thrust ($\overline{C_T} = 1.29$) is approximately 4 ($\overline{(\cdot)}$ denotes average over stroke). This factor is in reasonable agreement with the forces measured experimentally (Drucker & Lauder, 2001).

Returning to Figure 7(a), we note that the C_Z peak is reached between $t/T = 0.15$ and $t/T = 0.3$. Shortly thereafter, the C_T peak occurs between $t/T = 0.3$ and $t/T = 0.4$. As expected, the first priority in the maneuver is to evade the stimulus (an obstacle or predator in the wild) by quickly generating a strong lateral force (maximum occurs at $t/T = 0.2$). Thereafter, the drag force developed in the streamwise direction is likely used to modulate the

FIGURE 7

Comparison of time variation of force coefficients: (a) strongside and (b) weakside.



direction of the resultant force as the sunfish turns away from the stimulus. The evolving vortex ring, clearly seen in Figures 8(d) and 8(f), continues to be oriented nearly parallel to the fish body. Consequently, the lateral jet orientation ensures that the maximum lateral force continues to act normal to the fish body for the duration of the maneuver. Here, the inherent flexibility of the pectoral fin structure and the ability to continuously alter planform area is likely to be very useful.

Finally, an examination of the force histories for the dissected fin reveals that the peak lateral thrust developed by the dorsal part (rays 1-8) is approximately 70% of the total as opposed to 30% for the ventral (rays 8-14) portion (see Figure 10 and Figure 11c). The streamwise drag is slightly more comparable, although the dorsal part peak is higher (see Figure 11a). Overall, while the dorsal portion contributes to the majority of lateral force production, the ratio of dorsal to ventral contribution appears to be more equitable than the steady swimming case.

Conclusions

A comparative analysis of the pectoral fin performance in steady swim-

ming and yaw turn maneuver reveals that the dorsal part of the pectoral fin is responsible for the majority of force production. The chordwise and spanwise flexibility of the pectoral fin and its ability to have them function either in concert or independently seems to enable the bluegill sunfish to achieve a variety of maneuvers. The virtual dissection reveals a significant loss of performance with maneuvering with respect to peak lateral thrust when the ventral portion is removed. Thus, a fin design using just the dorsal portion of the pectoral fin might perform as well as the full fin in steady swimming but will not retain the same maneuverability. Hence, any effective design based on the pectoral fin that aims to preserve its performance over all locomotion mode needs to retain a greater portion of the fin than that suggested by steady swimming alone.

The pectoral fins of fishes display a diversity of shapes (e.g., Drucker & Lauder, 2002; Thorsen & Westneat, 2005), and although some general conclusions about correlations of fin shape with fish ecology have been possible (see Wainwright et al., 2002), there are very few data on functional regionalization of pectoral fins and on the role that different fin rays within

FIGURE 8

Formation of the vortex ring due to the strongside pectoral fin motion: (a), (c), and (e) are lateral views at $t/T = 0.22$, $t/T = 0.49$, and $t/T = 0.66$, respectively; (b), (d), and (f) are the corresponding dorsal views at $t/T = 0.22$, $t/T = 0.49$, and $t/T = 0.66$, respectively.

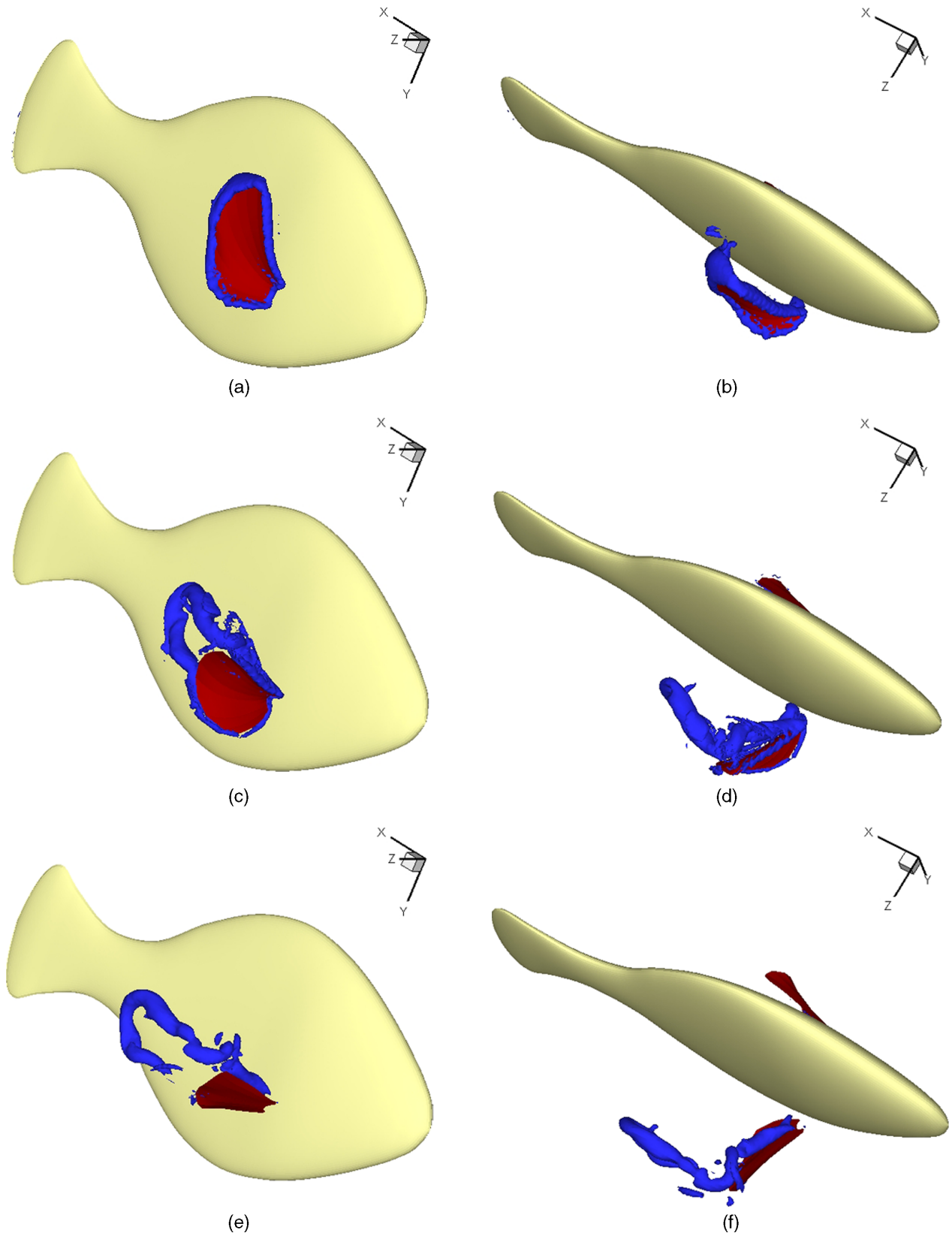


FIGURE 9

The strongside lateral jet associated with the vortex structures in Figure 8 (c) at $t/T = 0.49$.

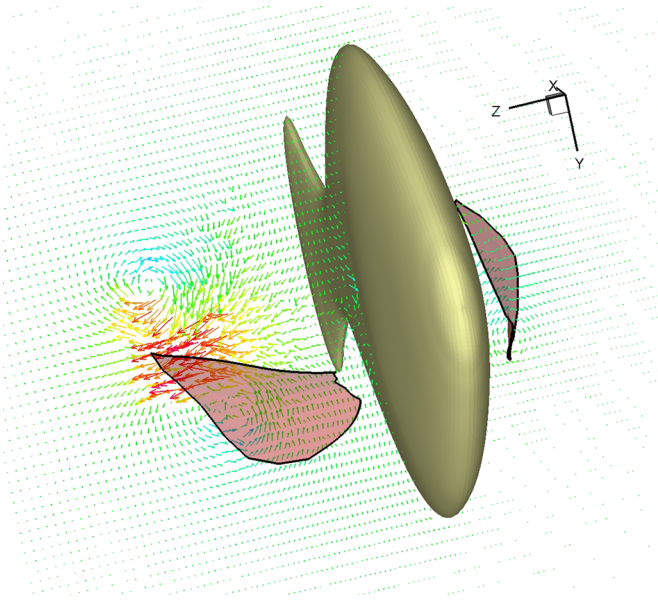


FIGURE 10

Formation of the vortex ring due to the strongside pectoral fin motion: (a) full, (b) dorsal, and (c) ventral portion of the fin sections.

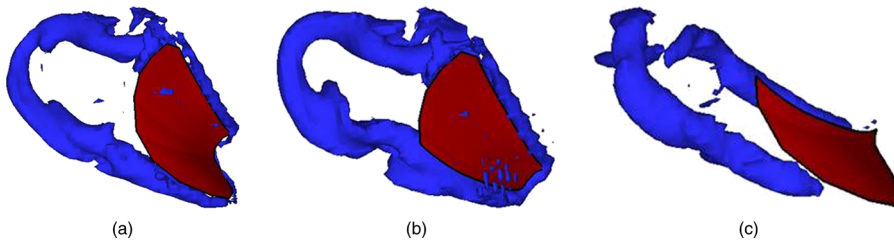
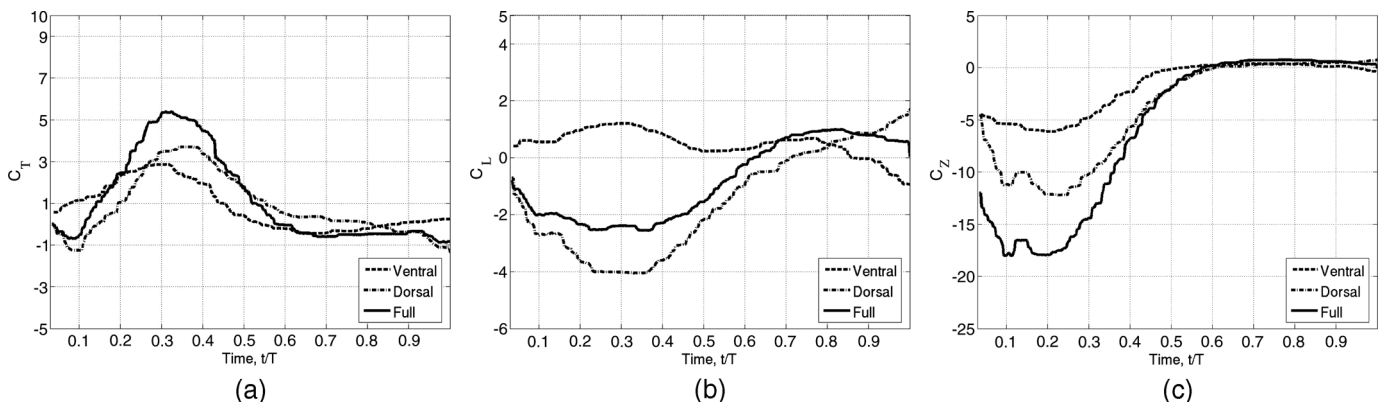


FIGURE 11

Comparison of forces produced on the dorsal and ventral halves of the strongside fin with respect to the full fin: (a) streamwise force, (b) vertical force, and (c) lateral force.



the pectoral fin might play in controlling locomotor performance. Taft et al. (2008) discussed functional regionalization during steady swimming in sculpin, but the role that different fin rays play during maneuvering behaviors has not previously been analyzed. The results presented here suggest that the ventral region of the fin plays an important role in modulating maneuvering forces, and future studies on the diversity of fish pectoral fin shapes could focus on the surface area and mechanical properties of this region of the fin in correlation with maneuvering performance. No data are currently available that would permit even general conclusions about the diversification of pectoral fin structure in relation to maneuvering capability, and this represents a new and very interesting direction for future work that integrates approaches from biomechanics and fluid dynamics with behavioral and ecological studies of fish locomotion.

Acknowledgments

This work was done while the first three authors were at The George

Washington University, and the work was supported under ONR-MURI grant N00014-03-1-0897 monitored by Dr. Thomas McKenna.

Lead Author:

Srinivas Ramakrishnan
ANSYS, Inc.
10 Cavendish Court,
Lebanon, NH 03766
Email: srinivas.ramakrishnan@
ansys.com

References

- Akhtar**, I., Mittal, R., Lauder, G.V., & Drucker, E.G. 2007. Hydrodynamics of a biologically inspired tandem flapping foil configuration. *Theor Comp Fluid Dyn.* 21:155-70. doi: 10.1007/s00162-007-0045-2.
- Bozkurttas**, M. 2007. Hydrodynamic performance of fish pectoral fins with application to autonomous underwater vehicles. Ph.D. Thesis, The George Washington University. p. 9.
- Bozkurttas**, M., Mittal, R., Dong, H., Lauder, G.V., & Madden, P. 2009. A low-dimensional models and performance scaling of a highly deformable fish pectoral fin. *J Fluid Mech.* 631:311-42. doi: 10.1017/S0022112009007046.
- Chorin**, A.J. 1967. A numerical method for solving incompressible viscous flow problems. *J Comput Phys.* 2:1-9. doi: 10.1016/0021-9991(67)90037-X.
- Dong**, H., Bozkurttas, M., Mittal, R., Lauder, G.V., & Madden, P. 2010. A Computational modelling and analysis of the hydrodynamics of a highly deformable fish pectoral fin. *J Fluid Mech.* 645:345-73. doi: 10.1017/S0022112009992941.
- Dong**, H., Mittal, R., & Najjar, F.M. 2006. Wake topology and hydrodynamic performance of low-aspect-ratio flapping foils. *J Fluid Mech.* 566:309-43. doi: 10.1017/S002211200600190X.
- Drucker**, E.G., & Lauder, G.V. 2001. Wake dynamics and fluid forces of turning maneuvers in sunfish. *J Exp Biol.* 204:431-42.
- Drucker**, E.G., & Lauder, G.V. 2002. Experimental hydrodynamics of fish locomotion: Functional insights from wake visualization. *Integr Comp Biol.* 42:243-57. doi: 10.1093/icb/42.2.243.
- Lauder**, G.V., Madden, P.G.A., Mittal, R., Dong, H., & Bozkurttas, M. 2006. Locomotion with flexible propulsors: I. Experimental analysis of pectoral fin swimming in sunfish. *Bioinspir Biomim.* 1:35-41. doi: 10.1088/1748-3182/1/4/S04.
- Mittal**, R., Dong, H., Bozkurttas, M., & Lauder, G.V. 2006. Locomotion with flexible propulsors: II. Computational modeling of pectoral fin swimming in sunfish. *Bioinspir Biomim.* 1:25-34. doi: 10.1088/1748-3182/1/4/S05.
- Mittal**, R., Dong, H., Bozkurttas, M., Najjar, F.M., Vargas, A., & Von Loebbecke, A. 2008. A versatile sharp interface boundary method for incompressible flows with complex boundaries. *J Comput Phys.* 227:1-9. doi: 10.1016/j.jcp.2008.01.028.
- Mittal**, R., & Iaccarino, G. 2005. Immersed boundary methods. *Annu Rev Fluid Mech.* 37:239-61. doi: 10.1146/annurev.fluid.37.061903.175743.
- Osher**, S., & Sethian, J.A. 1988. Fronts propagating with curvature-dependent. *J Comput Phys.* 79:12-49. doi: 10.1016/0021-9991(88)90002-2.
- Taft**, N., Lauder, G.V., & Madden, P.G. 2008. Functional regionalization of the pectoral fin of the benthic longhorn sculpin during station holding and swimming. *J Zool Lond.* 276:159-67. doi: 10.1111/j.1469-7998.2008.00472.x.
- Thorsen**, D.H., & Westneat, M. 2005. Diversity of pectoral fin structure and function in fishes with labriform propulsion. *J Morphol.* 263:133-50. doi: 10.1002/jmor.10173.
- Tran**, L.B., & Udaykumar, H.S. 2004. A particle-level set-based sharp interface cartesian grid method for impact, penetration, and void collapse. *J Comput Phys.* 193:469-510. doi: 10.1016/j.jcp.2003.07.023.
- Wainwright**, P., Bellwood, D.R., & Westneat, M. 2002. Ecomorphology of locomotion in labrid fishes. *Environ Biol Fish.* 65:47-62. doi: 10.1023/A:1019671131001.
- Ye**, T., Mittal, R., Udaykumar, H.S., & Shyy, W. 1999. An accurate Cartesian grid method for simulation of viscous incompressible flows with complex immersed boundaries. *J Comput Phys.* 156:209-40. doi: 10.1006/jcph.1999.6356.
- Zang**, Y., Streett, R.L., & Koseff, J.R. 1994. A non-staggered fractional step method for time-dependent incompressible Navier-Stokes equations in curvilinear coordinates. *J Comput Phys.* 114:18-33. doi: 10.1006/jcph.1994.1146.